ELSEVIER

Surface Science 477 (2001) 209–218

SURFACE SCIENCE

www.elsevier.nl/locate/susc

Ordered alloy films of Ni and Mn grown on Ni(1 1 1)/W(1 1 0)

M.A.J. Allen, D. Venus *

Department of Physics and Astronomy and Brockhouse Institute for Materials Research, McMaster University, 1280 Main Street West, Hamilton, ON, Canada L8S 4M1

Received 8 November 2000; accepted for publication 11 January 2001

Abstract

Ultrathin films of alloyed Ni and Mn have been grown by depositing Mn on 4 ML Ni/W(1 1 0) and annealing to 550 K. Directional Auger electron spectroscopy (DAES) shows that the films have short-range structural order that is at most slightly distorted from the f.c.c. (1 1 1) structure of the Ni film. Low energy electron diffraction (LEED) shows that the films have long-range order due to chemical ordering of the Ni and Mn. Depending on the Ni:Mn ratio, the LEED and DAES are consistent with structures similar to bulk Ni_3Mn, bulk NiMn, and with a subsurface structure similar to the $(\sqrt{3} \times \sqrt{3})R30$, 2:1 surface alloy observed for Mn/Cu(1 1 1).

Keywords: Alloys; Nickel; Manganese; Single crystal epitaxy; Growth; Surface structure, morphology, roughness and topography; Auger electron diffraction; Low energy electron diffraction (LEED)

1. Introduction

The effects of surfaces and interfaces on the structural and magnetic properties of ferromagnetic films have been widely studied and have led to the description of intriguing phenomena such as oscillatory layer exchange, giant magnetoresistance and perpendicular magnetic anisotropy [1]. There has been a more modest effort to study the influence of surfaces and interfaces on antiferromagnetic films, in part because of the difficulty in extracting magnetic information from magnetically compensated surfaces, and in part because antiferromagnetic systems are often ordered alloys and the preparation of high quality films is more difficult. Over the last five years, the area has been given great impetus by the desire to understand the magnetic exchange coupling at an antiferromagnetic/ferromagnetic interface which gives rise to the exchange biased hysteresis loops in spin valves [2,3]. Most of these studies have been conducted on relatively thick films, where the influence of surfaces is not paramount. However, some recent work has demonstrated the role of interfaces in the stabilization of antiferromagnetic alloys which do not occur in bulk [4–6], perhaps because of large magnetic moments on the surface atoms. Other work illustrates the dependence of the Néel temperature upon film thickness [7,8], the effect of ferromagnetic boundary layers on the Néel temperature [9], and the observation of ferromagnetism in surface alloys which are antiferromagnetic in their bulk form [10,11].

The present work on the formation of Ni–Mn alloys in ultrathin films is of interest because

* Corresponding author. Tel.: +1-905-525-9140; fax: +1-905-546-1252.

E-mail address: venus@physics.mcmaster.ca (D. Venus).

0039-6028/01/$ - see front matter
PII: S0039-6028(01)00773-7

antiferromagnetic NiMn films are often used as pinning layers in spin valves [12], but also because of the many structural and magnetic phases which are observed in the bulk [13]. These include a range of alloys close to the composition Ni_3Mn which become ferromagnetic when chemically ordered, as well as alloys with composition close to NiMn which are paramagnetic in a cubic phase but antiferromagnetic in a tetragonal phase. The interplay of surface strain in epitaxy, high atom mobility at surfaces, and layer-dependent magnetic moments make it uncertain how these phases will be expressed at a surface, and offer an opportunity to study their effect on ultrathin alloy films. As a first step in investigating these questions, the present work looks at the structure of alloys formed by depositing Mn on f.c.c. Ni(1 1 1) grown on a W(1 1 0) single crystal, and then annealing the film. This system may also serve as a model for the growth of the (1 1 1) oriented Mn–Ni alloys used in spin valves.

Previous studies of thin Ni–Mn alloy films have been restricted to growth on the (0 0 1) face. These show that a buckled c(2×2) surface alloy forms at 0.5 monolayers (ML) Mn coverage on Ni(0 0 1) [14,15], much as is the case for Mn/Cu(0 0 1) [4]. This surface alloy is ferromagnetically coupled to the Ni(0 0 1) substrate [10,11]. Thicker alloy films of up to 4 ML grown on a Ni(0 0 1) single crystal form a tetragonal phase like bulk NiMn, except that the *c*-axis of tetragonal distortion is changed [10]. In bulk NiMn the *c*-axis spacing is compressed by 6% compared to the *ab* plane; when grown on Ni(0 0 1), the *a*-axis is compressed equivalent to the bulk *c*-axis to form a new $a'b'$ plane at right angles to the bulk *ab* plane. The undistorted c' axis is normal to the surface. The thicker films are also reported to be ferromagnetic [10]. Addition of further Mn creates an excess on the surface which forms a series of ordered surface structures [14].

Epitaxy of Ni–Mn alloys several atomic layers in thickness on Ni(1 1 1)/W(1 1 0) require much less distortion of the bulk structure. This is because the Ni substrate is itself 3% expanded compared to bulk Ni [16], and also because the entire misfit need not be taken up along a single principal axis. This situation is illustrated in Fig. 1. Fig. 1a shows

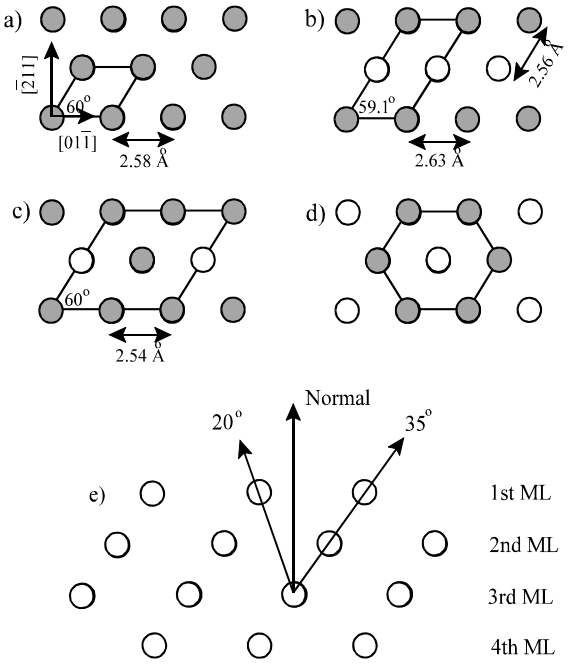

Fig. 1. The arrangement of surface atoms and the unit cell for planes in various structures. (a) Ni(1 1 1)/W(1 1 0), (b) tetragonal bulk NiMn(1 1 1), (c) bulk Ni_3Mn (1 1 1), (d) the $(\sqrt{3} \times \sqrt{3})R30$ surface alloy formed by Mn/Cu(1 1 1).

the surface unit cell of f.c.c. Ni(1 1 1)/W(1 1 0). In Fig. 1b the surface unit cell of bulk NiMn perpendicular to the body diagonal is given. It requires a 1.7% expansion along $[\bar{2}11]$ of the Ni substrate and a 1.9% compression along $[01\bar{1}]$ of the Ni substrate for epitaxy. Fig. 1c shows that of Ni_3Mn (1 1 1), which has the Cu_3Au structure and requires a uniform 1.6% expansion for epitaxial growth. Between these 1:1 and 3:1 stoichiometric alloys, bulk NiMn forms a continuous range of locally ordered alloys [13]. It is possible that the intermediate case of 2:1 stoichiometry may occur for Ni–Mn films, since it is observed for Mn films grown on the (1 1 1) faces of other metals, where it produces a $(\sqrt{3} \times \sqrt{3})R30$ structure at 1/3 ML coverage. Examples are Cu(1 1 1) [17,18], Pt(1 1 1) [19], Ir(1 1 1) [20] and h.c.p. Ru(0 0 0 1) [21]. For Mn/Cu(1 1 1) there is evidence that an alloy is formed [18]. It is not yet clear whether or not this alloy is restricted to the top Cu layer, but theoretical calculations suggest it is not [22]. The formation of thicker alloy on (1 1 1) surfaces may be

hindered by the lower mobility of atoms in this close-packed plane compared to the (0 0 1) surface [23]. The surface unit cell for a similar structure for Mn/Ni(1 1 1) is illustrated in Fig. 1d. Finally, Fig. 1e shows a cross-section of an f.c.c. (1 1 1) film for later reference.

The present study provides strong evidence that all three phases shown in Fig. 1 exist as surface and subsurface alloys, depending upon the ratio of Ni:Mn, and upon the gradient of this ratio as Mn moves from the surface to deeper into the Ni substrate upon annealing. Evidence for long-range ordering comes from low energy electron diffraction (LEED) and for short-range ordering and mixing of the Mn into the Ni comes from Auger electron spectroscopy (AES) and directional Auger electron spectroscopy (DAES). It appears that Mn/Ni(1 1 1)/W(1 1 0) is a good model in which to study the formation of Ni–Mn alloy films with a (1 1 1) orientation, and for further work investigating the relation between alloy structure and magnetic properties of films.

2. Experimental methods

2.1. Thickness calibration

The reliable growth of ultrathin films requires a careful calibration of the amount of evaporant which is deposited on the substrate. Since quartz crystal thickness monitors are not reliable at the level of 0.2 ML, it is usually necessary to study the growth of the films and find a reproducible marker which can be identified with a particular effective film thickness. In the present case, AES was used to monitor the growth of Mn on the bare W(1 1 0) substrate, and these results were compared to previous scanning tunnelling microscopy studies [24] to affect a calibration. The Mn was precleaned by vacuum evaporation at 10^{-6} Torr in a molybdenum tube, and the resulting brittle Mn plug was crushed. Mn pieces were placed in a basket made from a fine molybdenum wire mesh, and the basket was then spot welded to a 1 mm diameter Ta rod. This was then placed in an electron beam evaporation source [25] originally designed to evaporate the tip of a pure metal wire. Because of the high vapour pressure of Mn, only 5–10 W of power was required to evaporate at a rate of 1 ML in 5 min. The rate was kept constant by monitoring the current of Mn ions intercepted on the exit aperture of the evaporator [25]. During the evaporation, the pressure rose to the low 10^{-9} Torr range, but recovered quickly to the base pressure of 2×10^{-10} Torr.

Scanning tunnelling microscopy studies by Bode et al. [24] show that Mn grows epitaxially, but not layer by layer, on W(1 1 0) until an effective coverage of 1.3 ML. The film then nucleates three-dimensional growth on those portions of the surface that are locally three atoms thick. The authors provide figures giving the fractional surface coverage of each local thickness as a function of time. Using these, the expected attenuation of the substrate W signal in AES was calculated as a function of the total equivalent deposition, and is shown in Fig. 2a. The shape of the curve does not depend on the escape depth that is assumed. While the data describe a continuous curve, the change of growth morphology is evident when two straight lines are fit to the points. Despite the fact that no constraint is placed upon the endpoints of the lines, the best least-squares fit shown in Fig. 2a gives a break very near to 1.3 ML equivalent coverage where the change in growth morphology occurs.

Experimental measurements of the Auger electron signal from the substrate and the Mn film were made for a series of 30 s cumulative Mn depositions, both at the W NOO Auger peak (150–190 V) and the W and Mn core–valence Auger peaks (30–55 V). The W NOO spectra were fit to a W NOO spectrum from a clean substrate by scaling them with a coefficient that is plotted in Fig. 2b. Each core–valence spectrum $I(E)$ was fit to a linear combination of core–valence spectra from a clean W substrate $I_W(E)$ and a thick Mn film $I_{Mn}(E)$, as

$$I(E) = \alpha I_W(E) + \beta I_{Mn}(E). \quad (1)$$

The resulting fitting coefficients are plotted in Fig. 2c. The fits described the spectra very well, as is indicated by the error bars of the fitting coefficients derived from them. It is clear that both sets of data are also well represented by two straight

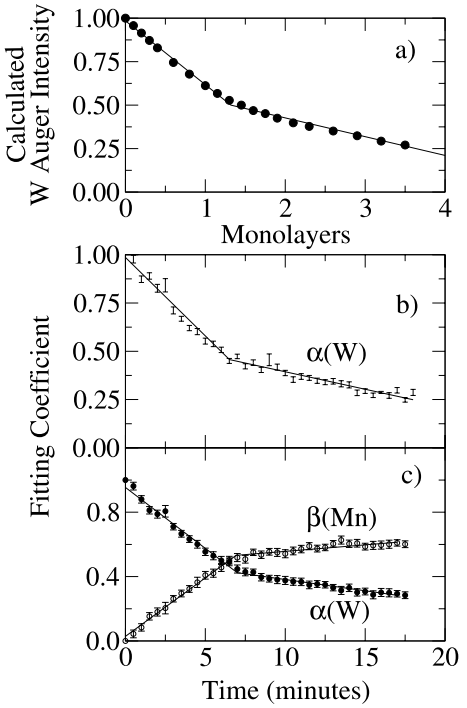

Fig. 2. Calibration of Mn deposition on W(1 1 0). (a) Intensity of 182 eV W Auger electrons calculated from the layer coverage data of Bode et al. [24]. (b) Experimental intensity of W Auger electrons in the energy range 150–190 eV as a function of the Mn deposition time at a constant deposition rate. The fitted coefficient which scales the spectrum to that of a clean W substrate is plotted. (c) As in (b), but for Mn and W peaks in the energy range from 35–60 eV. The fitting coefficients α and β from Eq. (1) are plotted.

lines and unconstrained fitting of these lines places a break point between 6.0 and 6.5 min of deposition. The only free parameter in comparing the calculation in Fig. 2a and the data in Fig. 2b is the escape depth, d, of the Auger electrons. Optimizing this parameter for the best agreement gives $d = 4.5 \pm 0.2$ Å. In order to compare this value to the expected inelastic mean free path, λ, it must first be corrected by a geometrical factor for the acceptance angle of the retarding field analyser [26], and then for the effects of elastic scattering [27]. The result is $\lambda_{exp} = 7.2 \pm 0.8$ Å, which is to be compared to the theoretical value [28] of $\lambda_{theor} = 6.1 \pm 0.6$ Å for bulk Mn at 180 eV. This is acceptable agreement given the approximations involved in converting from escape depth to inelastic mean free path, and confirms that the analysis is self-consistent. The scales in Fig. 2a have been chosen using the optimized value of the escape depth, so that the calculated and experimental curves can be compared directly. For this experiment, 5 minutes of evaporation gives a Mn deposit equivalent to 1 ML. The data and calculated points are then indistinguishable within the experimental error bars when they are overplotted. Using the data of Fig. 2, the Mn ion flux on the aperture of the evaporator may be quickly calibrated in nA min/ML on W(1 1 0).

4 ML Ni films were used as a substrate for the deposition of Mn in this study. Ni films were grown on the W substrate using a procedure [29] which includes annealing the film after 1 ML to ensure good wetting. These substrates showed a hexagonal LEED pattern from two domains of f.c.c. (1 1 1) growth, in agreement with previously published results [16]. The thickness calibration for growth of Mn on the Ni film is made by adjusting by a factor of 1.3 to account for the different atom densities on b.c.c. (1 1 0) and f.c.c. (1 1 1) surfaces.

2.2. Directional Auger electron spectroscopy

In order to measure short-range order and to follow the possible formation of alloys in subsurface layers, DAES was used [30,31]. This is a variation on the better known technique of angle-resolved Auger electron spectroscopy [32], both of which use the focussing of electrons by near-neighbour atoms to infer the near-neighbour bond directions in a film. In DAES, the incoming electron beam of 1–3 keV is deflected by the positive ion cores. If it enters along a line of near-neighbour atoms, for example along the lines in Fig. 1e at 35° or 20° to the surface normal, then the beam is focussed toward other atoms along this line. These atoms then have a greater probability of Auger excitation. Because of the short inelastic mean free path of the Auger electrons, the external current of Auger electrons will be dominated by those created in the first few layers of the film. These outgoing Auger electrons will also be focussed by interaction with ion cores. However, if the Auger electrons are detected using a retarding field analyser with a large angle of acceptance, the

focussing effect on the outgoing electrons will be averaged out, leaving only the focussing effect upon the incoming electron beam. Measuring the Auger signal as a function of the orientation of the incoming beam then reveals peaks which indicate the directions of nearest-neighbour atoms.

DAES can provide a great deal of information about the structure of a film using only a simple qualitative analysis. In the first place, the existence of peaks shows that the film is ordered, and the angular positions of the peaks reveals the crystal structure. (The method is not exact enough to determine precise bond angles.) DAES is atom specific because the intensity of particular Auger transitions is measured. Furthermore, it is to some degree site specific, as can be seen from Fig. 1e. Atoms in the surface layer produce no peaks, those in the subsurface layer produce peaks only when the polar angle of incidence $\theta = 35°$ or 55°, and those two layers deep produce additional peaks when $\theta = 20°$ or 70°.

DAES profiles were measured as a function of the angle ϕ, the rotation of the film about its normal, for a fixed polar angle θ. This method ensured that the illumination of the retarding field analyser does not change within each scan at constant θ. The signal was collected in the d^2I/dV^2 mode using a lock-in amplifier, a stepping motor for azimuthal rotation, a time constant of 2 s, and an angular step of 2°. A single scan requires approximately 25 min. In order to remove the effect of the secondary electron background, the difference of scans recorded at the top and bottom of characteristic differentiated Auger peaks are presented. Results for a 4 ML Ni(1 1 1)/W(1 1 0) film are shown in Fig. 3 as the deviation from the mean Auger signal. The right hand panel was measured at the 60 eV Ni transition, and the left hand panel was measured at the 854 eV Ni transition. Measurements for different polar angles of incidence of the exciting electron beam appear in horizontal rows. For $\theta = 0$, the electron beam is incident along the axis of azimuthal rotation, and there should be no variation in the angle of beam incidence and no peaks. This data serves as a measure of the DAES signal that results from counting noise, misalignment of the axis of rotation, and other spurious effects. The measurements at

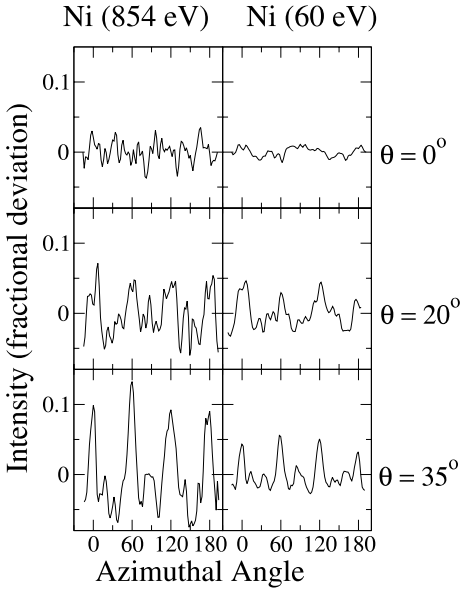

Fig. 3. DAES of 4 ML Ni(1 1 1)/W(1 1 0), presented as a fractional deviation from the mean Auger signal as a function of the sample rotation about its normal. Each column of graphs corresponds to a different Auger electron peak of Ni. Each row of graphs corresponds to a different angle of incidence of the primary beam.

$\theta = 35°$ and 20° show clear peaks due to focusing on Ni atoms below the surface layer, and below the top two surface layers, respectively. As can be seen from Fig. 1e, these peaks are expected every 120° starting at $\phi = 0$ for one f.c.c. (1 1 1) domain. The presence of two structural domains gives peaks every 60°. The higher energy Auger transition gives peak contrast of 10–15%, and the lower energy transition gives better signal-to-noise but less contrast. Minor reproducible peaks are due to second-order scattering, and more distant neighbours which are off axis and give only partial focusing.

The small peak at $\theta = 35°$, $\phi = 90°$ is not fully understood. There is a very strong focussing peak (40% deviation from mean Auger signal) for the b.c.c. W(1 1 0) substrate in this orientation [33]. This peak alone persists in the secondary electron background, for example, when the spectrometer is tuned to the energy of 300 V, well away from any W Auger peaks, and is not entirely removed from the Ni data by taking traces at the top and

bottom of the Ni Auger line and subtracting them. It may arise through a modulation of the secondary electron background by strong focussing within the top few layers of tungsten. It becomes most prominent in cases where there is a small Auger signal, since the DAES data is presented as a normalized deviation.

3. Results and discussion

3.1. Low energy electron diffraction and Auger electron spectroscopy

Experiments to study the formation of Ni–Mn alloys used a 4 ML Ni(1 1 1)/W(1 1 0) substrate upon which Mn was deposited. Fig. 4 presents the LEED patterns that result from various methods of preparation. Fig. 4a shows the LEED pattern for the 4 ML Ni substrate, and illustrates that the well known reconstructions that occur for thinner films are no longer present at this thickness [16]. Fig. 4b shows that the deposition of 0.5 ML of Mn on the Ni substrate at room temperature is sufficient to completely remove the LEED pattern. (The remaining spot, which is visible in many of the pictures, is due to a particle caught in the LEED optics.) This is different from many other Mn systems [19–21], where an ordered overlayer forms already at room temperature. In order to promote the formation of ordered alloys, the films were annealed after depositing the Mn.

An Auger electron spectroscopy study aimed at determining appropriate annealing conditions is presented in Fig. 5. A 1 ML Mn/4 ML Ni/W(1 1 0) film was annealed to successively higher temperatures for 1 min and Auger spectra were collected after each annealing step in the range of energies where all three elements have Auger transitions (35–60 eV). Each spectrum was fit to a linear combination of three basis spectra: $I_W(E)$ for clean W(1 1 0), $I_{Ni}(E)$ for 4 ML Ni/W(1 1 0), and $I_{Mn}(E)$ for 1 ML Mn/4 ML Ni/W(1 1 0), as

$$I(E) = \alpha I_W(E) + \beta I_{Mn}(E) + \gamma I_{Ni}(E). \quad (2)$$

The fitting coefficients are plotted as a function of annealing temperature, with the error bars in

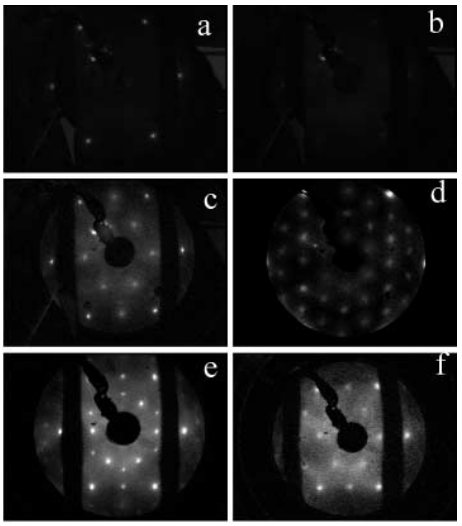

Fig. 4. LEED patterns of differently prepared surfaces. (a) 4 ML Ni/W(1 1 0) substrate for subsequent depositions, imaged with $E = 98$ eV (b) 0.5 ML Mn, not annealed, imaged with $E = 98$ eV (c) 0.5 ML Mn, annealed, imaged with $E = 91$ eV (d) 1.0 ML Mn, annealed, imaged with $E = 61$ eV (e) 1 ML Mn, annealed, imaged with $E = 125$ eV (f) 2.0 ML Mn, annealed, imaged with $E = 112$ eV.

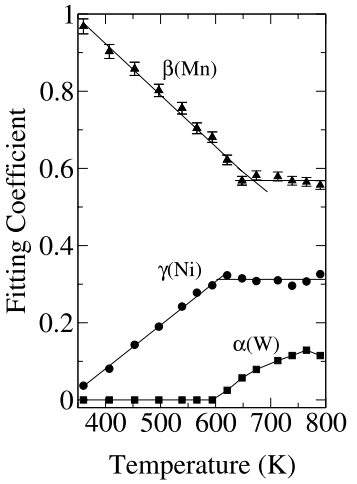

Fig. 5. The effect of annealing upon a 1 ML Mn/4 ML Ni/W(1 1 0) film. Auger electron spectra in the energy range 35–60 eV were recorded as a function of annealing temperature, and then fit to a linear combination of the spectra for clean W(1 1 0), 4 ML Ni/W(1 1 0) and 1 ML Mn/4 ML Ni/W(1 1 0). The coefficients α, β, γ from the least squares fit in Eq. (2) are plotted as a function of the annealing temperature.

two out of three cases as small as the plotting symbols. For low annealing temperatures there is no contribution from the W substrate, but the reduction in the Mn signal coupled with the increase in the Ni signal indicates that the Mn is mixing deeper into the film. Just above an annealing temperature of 600 K, there is a clear change in the curves. Auger electrons from W start to penetrate the film, while the Ni and Mn signals change very little. This is interpreted as the beginning of the breakup of the film, so that regions which are thinner allow the W substrate to be detected. It is reasonable that if the thermal energies are sufficient to cause larger mass transport, the Mn and Ni are completely mixed, and further annealing does not affect their Auger signals. This interpretation is corroborated by the observation of faint extra spots in the LEED pattern which are associated with the reconstruction of a thinner Ni film on W(1 1 0) [16]. As a result, an annealing temperature of 550 K was used in the rest of the study to promote alloy formation without causing degradation of the film integrity.

Returning to the LEED pictures in Fig. 4, it can be seen that annealing to 550 K for one minute gives not only a mixed Ni–Mn film, but one with long-range order. (Annealing for longer times did not affect the LEED pattern.) The annealed 0.5 ML Mn film (Fig. 4c) is seen to have a $p(2 \times 2)$ pattern when viewed with an electron beam energy less than about 170 eV. At higher beam energies, the superstructure spots are too faint to be seen. Annealing a 1 ML Mn film produces a $(2\sqrt{3} \times 2\sqrt{3})R30$ pattern (Fig. 4d) when using an electron beam energy up to 100 eV, beyond which the pattern is modified to become that shown in Fig. 4e. Annealing a 2 ML Mn film results once again in a $p(2 \times 2)$ pattern (Fig. 4f). At beam energies below 90 eV, there is a faint indication of the $(2\sqrt{3} \times 2\sqrt{3})R30$ pattern. Because it seems unusual to have a different LEED pattern at the intermediate coverage of 1 ML than for more or less Mn deposition, these results were reproduced many times. The $(2\sqrt{3} \times 2\sqrt{3})R30$ pattern was seen to exist roughly from 0.9 to 1.5 ML coverage.

Because the bulk phase diagram [13] indicates that chemically ordered alloys can be formed from disordered ones by heating above a certain threshold temperature and cooling, it is natural to attempt to understand these LEED patterns in terms of the bulk phases illustrated in Fig. 1. An ordered epitaxial layer with the nominal structure of NiMn would yield a $p(2 \times 1)$ pattern for the single domain in Fig. 1b, and a $p(2 \times 2)$ pattern from a collection of symmetry related domains. A layer with the nominal structure of Ni_3Mn in Fig. 1c would also give a $p(2 \times 2)$ LEED pattern. These two possibilities cannot therefore be distinguished. An interesting speculation is that the $(2\sqrt{3} \times 2\sqrt{3})R30$ pattern results from the coherent superposition of a $p(2 \times 2)$ pattern and the $(\sqrt{3} \times \sqrt{3})R30$ pattern illustrated in Fig. 1d, and seen for Mn films on other f.c.c. (1 1 1) substrates. To obtain a coherent superposition would require different layers which individually have each pattern, and suggests a gradient in the Mn concentration. Strong support for this hypothesis comes from Fig. 4e, taken at higher energy where multiple scattering is less important. Here many of the LEED spots disappear, leaving only those which are an incoherent superposition of a $p(2 \times 2)$ and $(\sqrt{3} \times \sqrt{3})R30$ pattern. In order to test these speculations, and resolve ambiguities, a probe of local structure, such as DAES, is required.

3.2. Directional Auger electron spectroscopy

DAES scans were taken before and after annealing the films using the higher energy Auger transitions of Mn and Ni, and angular settings of $\theta = 35°$ and 20°. Fig. 6 shows representative measurements for the unannealed films at $\theta = 35°$, for a 2 ML Mn deposition. The Mn DAES shows only a noisy signal, very similar to the spurious effects in Fig. 3 at $\theta = 0$. It is apparent that the Mn does not show focussing effects. Since the keV primary electrons used in these measurements are insensitive to the difference between Ni and Mn scattering potentials, this null result must be due to local structural disorder, and not merely chemical disorder. The Ni DAES, on the other hand, continues to show the characteristic peaks for an f.c.c. lattice seen for the clean Ni film. The definition and size of the peaks has been degraded by the upper layers of disordered Mn. The peak at $\phi = 90°$ discussed earlier is prominent in this trace

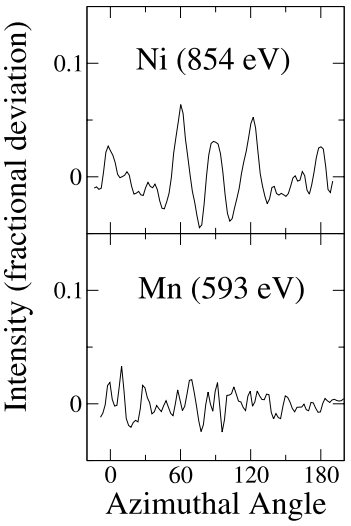

Fig. 6. DAES profiles at Ni and Mn Auger transitions, taken at $\theta = 35°$ from a 2 ML Mn film deposited at room temperature on 4 ML Ni/W(1 1 0). The profiles were measured before annealing the film.

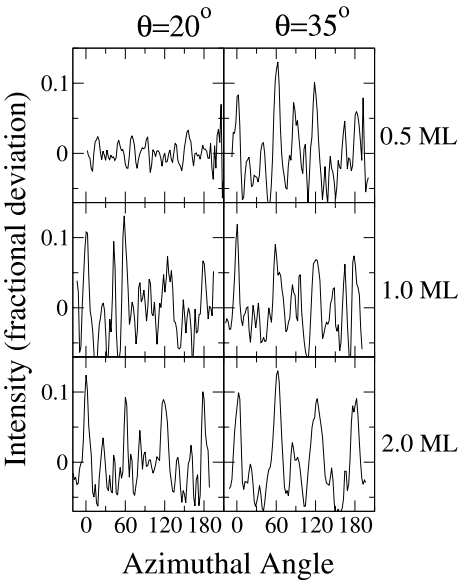

Fig. 7. DAES profiles at the 593 eV Mn Auger transition taken for various films after annealing to 550 K for 1 min. Each column of graphs corresponds to a different angle of the primary beam incidence. Each row of graphs corresponds to different deposits of Mn on 4 ML Ni/W(1 1 0).

because the f.c.c. Ni peaks are small, but is in fact the same size (~6%) as in the DAES profile for Ni/W(1 1 0). These findings support the earlier LEED and Auger studies. Disordered Mn lies on the top of the Ni when deposited at room temperature.

Upon annealing, the DAES of all the alloys show short-range f.c.c. order for both Ni and Mn atoms. In combination with the LEED patterns, this is strong evidence that ordered alloys are being formed. The Ni measurements are similar to those in Fig. 3, and are not shown here. The Mn measurements are given in Fig. 7. For the annealed film with 0.5 ML Mn in the top row of the figure, there are clear f.c.c. focussing peaks at $\theta = 35°$, but none at $\theta = 20°$. This must mean that many Mn atoms have one atomic layer of film above them, but none have two atomic layers above them. This immediately indicates that these films do not form a 1:1 NiMn surface layer alloy, as is the case for Mn/Ni(1 0 0) [15], Mn/Cu(1 0 0) [4], or Mn/Cu(1 1 0) [6]. Two simple models which are consistent with the DAES and p(2 × 2) LEED patterns are: two layers similar to the bulk Ni_3Mn structure in Fig. 1c, or one subsurface layer of 1:1 alloy similar to NiMn in Fig. 1b. Given the evidence for a Mn concentration gradient, only the first of these is reasonable.

Moving to the bottom row of DAES results in Fig. 7, the annealed film with a 2 ML Mn deposition shows f.c.c. focussing peaks at both $\theta = 35°$ and $\theta = 20°$. This indicates that the Mn penetrates at least two layers below the surface layer. Now the DAES and p(2 × 2) LEED are consistent with 4 ML of 1:1 NiMn, or a combination of NiMn near the surface and Ni_3Mn deeper into the film. (There is too much Mn to form uniform Ni_3Mn.)

The DAES measurements for the intermediate case of a 1 ML deposit of Mn show clear focussing peaks at $\theta = 35°$, but the focussing peaks at $\theta = 20°$, while certainly present, are not as clearly defined as for the case of a 2 ML deposit. This is interpreted as evidence that Mn penetrates at least two layers below the surface, but that there are fewer atoms in these positions than is the case for the 2 ML Mn film. This, in conjunction with the $(2\sqrt{3} \times 2\sqrt{3})R30$ LEED pattern, implies that the top layer is the 1:1 NiMn structure and the next layer is the 2:1 arrangement in Fig. 1d. This ac-

counts for an amount of Mn equal to 5/6 ML. A small amount of Mn likely penetrates deeper.

4. Conclusions

Ni–Mn alloy films with a structure close to f.c.c. (1 1 1) can be created by annealing Mn deposits on a Ni(1 1 1)/W(1 1 0) substrate to 550 K. Mn deposited at room temperature is disordered and does not appear to mix appreciably into the Ni layer. Upon annealing, AES indicates intermixing of the Mn and Ni, and DAES shows that all the alloys that are formed have a local structure which is at most a small distortion of f.c.c. (1 1 1) grown epitaxially on the Ni layer. LEED indicates that the alloys also have long-range order. This is most readily understood as chemical ordering, where the ordered alloy which is formed depends on the ratio of Ni:Mn and the gradient in that ratio. An annealed deposit of 0.5 ML Mn forms 2 ML consistent with the Ni_3Mn bulk structure, whereas an annealed deposit of 2.0 ML Mn forms about 4 ML consistent with the NiMn bulk structure. Because both of these structures require only small distortions (1.5–2.0%) from known bulk structures, these findings are consistent with a reasonable extrapolation of known data. However, the present experiments do not preclude other structures which are more speculative. Future quantitative LEED studies will be used to reach a definitive conclusion.

The intermediate case of annealing a 1 ML Mn deposit produces results not anticipated from the bulk phase diagram. The resulting $(2\sqrt{3} \times 2\sqrt{3})R30$ structure is best understood as a top layer of $p(2 \times 2)$ NiMn and a second layer of the $(\sqrt{3} \times \sqrt{3})R30$ structure observed when Mn is deposited on other f.c.c. (1 1 1) crystal faces. This 2:1 ordered alloy was not observed alone, and may be a metastable alloy which is formed only when the stoichiometry and a concentration gradient driven by diffusion does not permit the bulk alloys to form. It would be interesting to attempt to prepare films of this alloy alone, perhaps by annealing of sequential depositions of Ni and Mn of the correct stoichiometry, or by co-evaporation.

It appears that this system will provide an effective means to study how the bulk phase diagram of Ni–Mn alloys is expressed in ultrathin films with a f.c.c. (1 1 1) epitaxy. It will be particularly interesting to investigate the magnetic properties of these films to see what effect the surfaces and interfaces have on the corresponding change from ferromagnetic to antiferromagnetic ordering in the bulk phase diagram as the Mn concentration increases, and to see if they provide an effective model for investigating the exchange biasing of ferromagnetic films grown on NiMn (1 1 1).

Acknowledgements

This work was supported by the Natural Sciences and Engineering Research Council of Canada.

References

[1] B. Heinrich, J.A.C. Bland (Eds.), Ultrathin Magnetic Structures I and II, Springer, Berlin, 1994.
[2] A.E. Berkowitz, K. Takano, J. Magn. Magn. Mat. 200 (1999) 552.
[3] J. Nogués, I. K Schuller, J. Magn. Magn. Mat. 192 (1999) 203.
[4] M. Wuttig, Y. Gauthier, S. Blügel, Phys. Rev. Lett. 70 (1993) 3619.
[5] M. Wuttig, S. Junghans, T. Flores, S. Blügel, Phys. Rev. B 53 (1996) 7551.
[6] Ch. Ross, B. Schirmer, M. Wuttig, Y. Gauthier, G. Bihlmayer, S. Blügel, Phys. Rev. B 57 (1998) 2607.
[7] T. Ambrose, C.L. Chien, Phys. Rev. Lett. 76 (1996) 1743.
[8] X.W. Wu, C.L. Chien, Phys. Rev. Lett. 81 (1998) 2795.
[9] P.J. van der Zaag, Y. Ijiri, J.A. Borchers, L.F. Feiner, R.M. Wolf, J.M. Gaines, R.W. Erwin, M.A. Verheijen, Phys. Rev. Lett. 84 (2000) 6102.
[10] W.L. O'Brien, B.P. Tonner, Phys. Rev. B 51 (1995) 617.
[11] D. Schmidtz, O. Rader, C. Carbone, W. Eberhardt, Phys. Rev. B 54 (1996) 15,352.
[12] T. Lin, D. Mauri, N. Staud, C. Hwang, J.K. Howard, G.L. Gorman, Appl. Phys. Lett. 65 (1994) 1183.
[13] H.P.J. Wijn (Ed.), Magnetic Properties of Metals, vol. III/19a of the Landolt-Börnstein series, Springer, Berlin, 1986.
[14] M. Wuttig, T. Flores, C.C. Knight, Phys. Rev. B 48 (1993) 12,082.
[15] M. Wuttig, C.C. Knight, T. Flores, Y. Gauthier, Surf. Sci. 292 (1993) 189.
[16] K.P. Kämper, W. Schmitt, G. Güntherodt, Phys. Rev. B 38 (1998) 4951.

[17] D. Tian, A.M. Begely, F. Jona, Surf. Sci. Lett. 273 (1992) L393.
[18] J. Schneider, A. Rosenhahn, K. Wandelt, Appl. Surf. Sci. 142 (1999) 68.
[19] D. Tian, H. Li, S.C. Wu, F. Jona, Phys. Rev. B 45 (1992) 3749.
[20] W.L. O'Brien, B.P. Tonner, J. Vac. Sci. Technol. A 13 (1995) 1544.
[21] A.S. Arrot, B. Heinrich, S.T. Purcell, J.F. Cochran, K.B. Urquhart, J. Appl. Phys. 61 (1987) 3721.
[22] G. Bihlmayer, Ph. Kurz, S. Blügel, Phys. Rev. B 62 (2000) 4726.
[23] H. Ibach, M. Giesen, T. Flores, M. Wuttig, G. Treglia, Surf. Sci. 364 (1996) 453.
[24] M. Bode, M. Hennefarth, D. Haude, M. Getzlaff, R. Wiesendanger, Surf. Sci. 432 (1999) 8.
[25] T. Jones, J. Sawler, D. Venus, Rev. Sci. Instrum. 64 (1993) 2008.
[26] A. Jablonski, H. Ebel, Surf. Int. Anal. 11 (1988) 627.
[27] A. Jablonski, Surf. Sci. 188 (1987) 164.
[28] S. Tanuma, C.J. Powell, D.R. Penn, J. Vac. Sci. Technol. A 8 (1990) 2213.
[29] H.L. Johnston, C.S. Arnold, D. Venus, Phys. Rev. B 55 (1997) 13,221.
[30] S. Mróz, Surf. Rev. Lett. 4 (1997) 117.
[31] S. Mróz, M. Mowicki, Surf. Sci. 297 (1993) 66.
[32] W.F. Egelhoff Jr., in: J.A.C. Bland, B. Heinrich (Eds.), Ultrathin Magnetic Structures I, Springer, Berlin, 1994.
[33] M.A.J. Allen, Structural determination of ultrathin NiMn alloy films, M.Sc. Thesis, McMaster University, 2000.